

Magnetospheric convection and magnetopause shadowing effects in ULF wave-driven energetic electron transport

A. W. Degeling,¹ R. Rankin,¹ K. Murphy,¹ and I. J. Rae¹

Received 3 September 2012; revised 21 February 2013; accepted 6 March 2013; published 3 June 2013.

[1] Magnetospheric radiation belt electron transport in the presence of ULF waves and a convection electric field is investigated using a model that includes a nightside plasma sheet source and electron losses by magnetopause shadowing. Narrow-band ULF waves launched from a prescribed dayside magnetopause source are shown to interact with trapped and untrapped equatorially mirroring electrons within the magnetosphere. For magnetic moments less than 8 keV/nT and a strong convection electric field (in the order of 5 mV/m), we find that a limb of untrapped plasma sheet electrons extending across the dayside magnetosphere into the afternoon sector provides a phase space density (PSD) source for injection to lower L-shells by ULF waves, causing a rapid enhancement in PSD. However, the same ULF wave activity gives rise to a rapid dropout in PSD for electrons with a higher magnetic moment or in the presence of a weaker convection electric field, since in this case the plasma sheet electrons escape through the magnetopause before they reach the afternoon sector. In their place, a lack of PSD, or PSD “holes” can be periodically injected from the magnetopause to lower L-shells by ULF waves, leading to the rapid depletion in average PSD. In each case, the magnitude and extent in L-shell of the PSD enhancement or depletion is strongly dependent on the amplitude of ULF waves in the afternoon sector, and is significantly augmented by the overlap of drift-resonant islands and an associated stochastic transport layer.

Citation: Degeling, A. W., R. Rankin, K. Murphy, and I. J. Rae (2013), Magnetospheric convection and magnetopause shadowing effects in ULF wave-driven energetic electron transport, *J. Geophys. Res. Space Physics*, 118, 2919–2927, doi:10.1002/jgra.50219.

1. Introduction

[2] A particular challenge in studying radiation belt electron dynamics is understanding the observed variability in the response of the radiation belts to apparently similar geomagnetic storms [O’Brien *et al.*, 2001; Friedel *et al.*, 2002]. In general, the state of the radiation belt at a given time is best understood in terms of particle conservation, and the adiabatic invariants [Northrop, 1963]: The phase space density (PSD) at a given location and set of invariant values is determined by conservative adiabatic transport, and local non-adiabatic effects that represent sinks or sources in PSD. For example, Hudson *et al.* [2008] review energization mechanisms, such as prompt and diffusive radial transport (breaking the third invariant), and local acceleration (breaking the first invariant) and loss mechanisms, such as pitch-angle scattering to the ionosphere (breaking the first or second invariants), or outward radial diffusion (breaking the third invariant) in the presence of a dynamically varying magnetopause boundary. Loto’aniu *et al.* [2010] and

Turner *et al.* [2012b] report examples of events where magnetopause shadowing and ULF wave-driven outward radial diffusion give rise to rapid radiation belt dropouts. In a survey of 52 events, Green *et al.* [2004] find that rapid relativistic electron depletions are initiated in the dusk sector, and are associated with the stretching of dusk sector magnetic field lines due to the formation of a partial ring current, and that the electron losses in these cases are most probably due to pitch-angle scattering to the ionosphere. Losses to the magnetopause are discounted in this study because the electron depletions occur at L-shells significantly lower than the minimum estimated magnetopause location (given by the model of Shue *et al.* [1997]).

[3] In previous work [Degeling and Rankin, 2008], coherent transport via the drift-resonant interaction with ULF waves was investigated as a potential rapid energization mechanism for radiation belt electrons. Several studies support an internal source of PSD that drives local acceleration at the heart of the inner belt [Brautigam and Albert, 2000; Green and Kivelson, 2004; Chen *et al.*, 2007; Shprits *et al.*, 2007; Koller *et al.*, 2007; Turner and Li, 2008; Turner *et al.*, 2010; Turner *et al.*, 2012a], however, Degeling and Rankin [2008] suggest that peaks in PSD in that location may also arise when the source is in the plasma sheet. In that work, a constant azimuthally symmetric source of electrons at high L-shell was assumed. In this article, we consider the scenario where the nightside plasma sheet

¹Department of Physics, University of Alberta, Edmonton, Alberta, Canada.

Corresponding author: A. W. Degeling, Department of Physics, University of Alberta, Edmonton, AB, Canada T6G 2G7. (degeling@ualberta.ca)

provides a constant source of electrons, and losses are permitted through the dayside magnetopause. This represents a logical next step from *Degeling and Rankin* [2008]; *Degeling et al.* [2011] before more complicated scenarios, such as the inclusion of time-dependent electron sources from either the plasma sheet or inner magnetosphere, can be considered. In particular, *Turner et al.* [2012a] concluded from THEMIS observations that a constant source of relativistic electrons was not present in the plasma sheet. However, they also noted that a time dependent source was not ruled out as THEMIS would not detect such a source.

[4] In this context, the impact of ULF wave activity is arguably most significant when the resulting transport links untrapped and trapped electron drift trajectories, in which case it is important to ask where the untrapped trajectories originate. For example, electron trajectories originating in the nightside plasma sheet provide an enhancement in PSD at lower L-shell. On the other hand, electron trajectories intersecting the magnetopause enable the transport of an absence of phase space density or “PSD hole”, and a radiation belt PSD depletion. The location of the last closed drift shell, in relation to the magnetopause and regions of ULF wave activity, therefore plays a pivotal role in determining whether ULF wave-driven transport enhances or depletes electron phase space density. This is demonstrated using a numerical model for ideal MHD waves within a magnetosphere including day/night asymmetry and a parabolic magnetopause to drive the adiabatic transport of equatorially mirroring electrons [*Degeling et al.*, 2011]. Narrow band ULF waves are launched from the dayside magnetopause and are found to most significantly perturb electron trajectories in the afternoon sector. Parametrically scanning the convection field strength ψ_0 , we find that ULF wave-driven transport can result in a rapid PSD depletion (dropout) for weak convection and a significant PSD enhancement for strong convection, depending on the magnitude of the magnetic moment M , ULF wave amplitude, and the location of the separatrix between trapped and untrapped electrons. The model results that are presented below predict PSD depletion across a range of M for ψ_0 less than 1 kV, and for M greater than 8 keV/nT for $\psi_0=3$ kV. This can be compared with statistical results from *Shprits et al.* [2012], which suggest that dropouts most often occur following pressure enhancements and correspondingly enhanced convection. Here, we present counter-examples based on a model of ULF waves and an observational database that shows dropouts when such waves are present. It is interesting to note that in the weak convection case, PSD depletions occur at L-shells significantly earthward of the mean magnetopause location, and are initiated in the dusk sector.

2. Electron Transport Model Overview

2.1. The ULF Wave and Convection Electric Field Models

[5] We use the 2D plus t finite element model described in [*Degeling et al.*, 2011] to calculate the perturbed electric and magnetic fields in the equatorial plane due to low frequency ideal MHD waves, assuming a box magnetic field geometry with a parabolic interface representing the magnetopause boundary. A brief review of the model is given here,

and we direct the interested reader to [*Degeling et al.*, 2011] for further details.

[6] Low frequency waves in the magnetosphere satisfying ideal MHD can be modeled by the following linear equations

$$\frac{\partial b}{\partial t} = -\nabla \times E \quad (1)$$

$$\frac{1}{v_A^2} \frac{\partial \mathbf{E}}{\partial t} = (\nabla \times \mathbf{b})_{\perp} - \frac{(\mu_o \mathbf{J} \times \mathbf{b}) \times B_o}{B_o^2} + \mu_o \mathbf{J}^{\text{ext}} \quad (2)$$

where B_o is the unperturbed geomagnetic field, $\mu_o \mathbf{J} = \nabla \times B_o$ is the associated current density, b and E are the perturbed magnetic and electric fields respectively, v_A is the Alfvén speed and \mathbf{J}^{ext} is a perpendicular current source term for launching waves. These equations describe the propagation across the magnetic field of MHD fast waves launched by the wave source described by \mathbf{J}^{ext} , and linear mode coupling to shear Alfvén waves on field lines where the fast mode wave frequency matches an eigenfrequency for standing waves. Locations where this occurs develop a characteristic peak and associated phase change in the equatorial electric field, and are known as field line resonances (FLRs) [*Rankin et al.*, 2006; *Allan and Knox*, 1979; *Allan and Poulter*, 1992; *Samson et al.*, 1971]. The values of unperturbed parameters in the model, such as those specifying the magnetopause shape and equatorial plasma density profile are left unaltered from those used in *Degeling et al.* [2011]. An effective field line length of $15R_E$ is used in this study. ULF waves with a driver frequency of 1 mHz are launched from the magnetopause boundary by arranging \mathbf{J}^{ext} to be strongly peaked across the boundary (FWHM of $1 R_E$) and broadly peaked along the boundary (FWHM of $5 R_E$), with a polarization to give magnetic field line displacements in the transverse direction. Two cases are studied in this paper: (a) morning and (b) afternoon ULF wave excitation, with \mathbf{J}^{ext} peaked at 0900 h and 1500 h *MLT* respectively. Figure 1 shows an example of the amplitude and phase of the radial and azimuthal electric fields for case (a), and case (b) corresponds to the reflection of Figure 1 about the noon meridian. This figure shows that the magnetopause disturbance launches MHD fast waves into the magnetosphere, which form a standing wave structure on the dayside, and propagate preferentially down the duskside flank. These waves couple to a field line resonance at approximately $L = 5$ (and preferentially in the afternoon sector), as evidenced by narrow structure in the radial electric field and an associated rapid phase change (not explicitly shown).

[7] The ULF wave model of *Degeling et al.* [2011] has been extended to solve the evolution of wave fields in response to temporal variations in the ULF wave source, using an implicit time integrator in conjunction with the FEM solver for the spatial dimensions. In all cases, the amplitude of the driver wave packet is given the form $\exp(-t/\tau_f)(1 - \exp(-t/\tau_r))$, with the rise time τ_r and decay time τ_f set to one and 10 wave periods, respectively.

[8] In order to include the effect of magnetospheric convection, we calculate the electrostatic potential Φ according to the model of *Volland* [1973] and *Stern* [1975], given by

$$\Phi = \psi_o L^2 \sin \phi - \frac{\Omega_E B_o E R_E^2}{L} \quad (3)$$

where ψ_o controls the strength of the convection field, ϕ is the azimuthal angle and L is the dimensionless L-shell

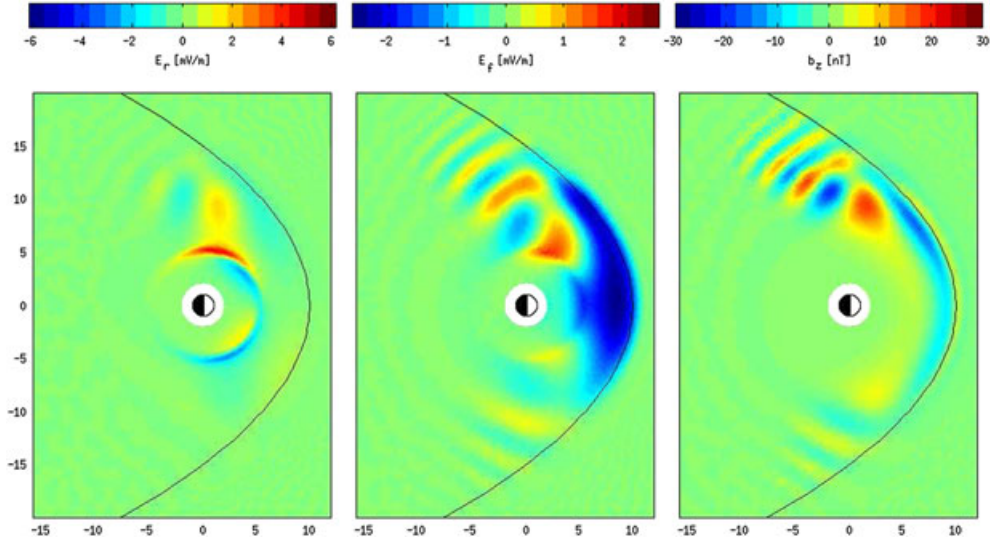


Figure 1. The ULF wave model outputs for a 1 mHz ULF wave source located along the afternoon sector magnetopause (peaked at 1500 h MLT), showing: E_r (mV/m) (left) E_ϕ (mV/m) (center) and b_z (nT) (right). These plots were taken five wave periods after the beginning of the source wave packet.

parameter, Ω_E , B_{oE} and R_E are the Earth’s angular rotation frequency, equatorial surface magnetic field strength and radius, respectively. For the purposes of this paper, L is given by $(B_{oE}/B(r, \phi, t))^{1/3}$. A value of $\psi_o = 3kV$ corresponds to a peak dawn-dusk convection electric field of about 5 mV/m. Typical observed values of the large scale convection electric field are less than 1 mV/m during quiet times and can peak around 6 mV/m during intense geomagnetic storms [Wygant *et al.*, 1998]. It is interesting to note that time dependence in the magnetic field strength due to ULF wave perturbations gives rise to time dependence in Φ . This corresponds to the oscillatory motion of magnetic field lines on which the electrostatic potential Φ is held constant. The convection/corotation electric field in the stationary frame is given by the gradient of Φ , and is therefore also time varying in response to the magnetic field perturbations—however, this electric field is curl-free.

2.2. Equatorially Mirroring Electron Transport Model Including Magnetopause Shadowing

[9] Taking the same approach as Degeling *et al.* [2011], we consider the simplified dynamics of equatorially mirroring electrons with constant first adiabatic invariant M , charge q and mass m_e , for which the guiding center equation of motion is [Northrop, 1963]

$$\mathbf{v} = \frac{\mathbf{E} \times \mathbf{B}}{B^2} + \frac{M}{q\gamma} \frac{\mathbf{B} \times \nabla B}{B^2} \quad (4)$$

where $\gamma = (1 + 2MB/m_e c^2)^{1/2}$ is the relativistic correction factor.

[10] The above equation is used to drive a test-kinetic simulation for markers of constant phase space density $f = f(r, \phi, M, t)$ within the magnetosphere. This is done by assuming an initial distribution of the form $f = f_o(L_o, M)$, where $L_o(r, \phi)$ is the initial L-shell value as a function of

position, and calculating the mapping of L_o to later times by solving the advection equation for $L_o = L_o(r, \phi, t)$:

$$\frac{\partial L_o}{\partial t} + \mathbf{v} \cdot \nabla L_o = 0 \quad (5)$$

This equation is solved numerically on a fixed polar coordinate grid using operator splitting and a 1-D flux corrected transport algorithm, with equation 4 calculated using fields interpolated from the ULF wave and convection models.

[11] We include particle loss through the magnetopause (magnetopause shadowing [West *et al.*, 1972]) by adding the rule for each time step in the calculation that $L_o(r, \phi, t) = 0$ for points outside the magnetopause boundary, and furthermore that $f_o(L_o, M) = 0$ for $L_o < 1$. That is, upon leaving the magnetosphere, L_o is assigned a value at which the phase space density is defined to be zero. This also ensures that any flows into the magnetosphere across the magnetopause boundary are assigned zero phase space density, and represent a “hole” in PSD. The location of the magnetopause boundary under the action of ULF waves is not stationary, but oscillates at the wave frequency ω in accordance with the ideal MHD displacement of field lines ξ , given by $-\omega \xi = (\mathbf{E} \times \mathbf{B})/B^2$. This motion is included in the above consideration of particle losses through the magnetopause.

3. Results: ULF Wave-Driven PSD Enhancement and Loss

[12] Figure 2 shows the time evolution in electron phase space density, with M set to 5 keV/nT, under the action of 1 mHz ULF waves launched from a source centered at 1500 h MLT (as shown in Figure 1). Each column in this figure corresponds to a different value of ψ_o in the Volland-Stern convection field model, increasing from left to right. In each case, the electron PSD was initialized with a Kappa distribution with $\kappa = 4$ and effective temperature of 15 keV, and allowed to transport under the action of the convection/corotation electric field only for an interval of about

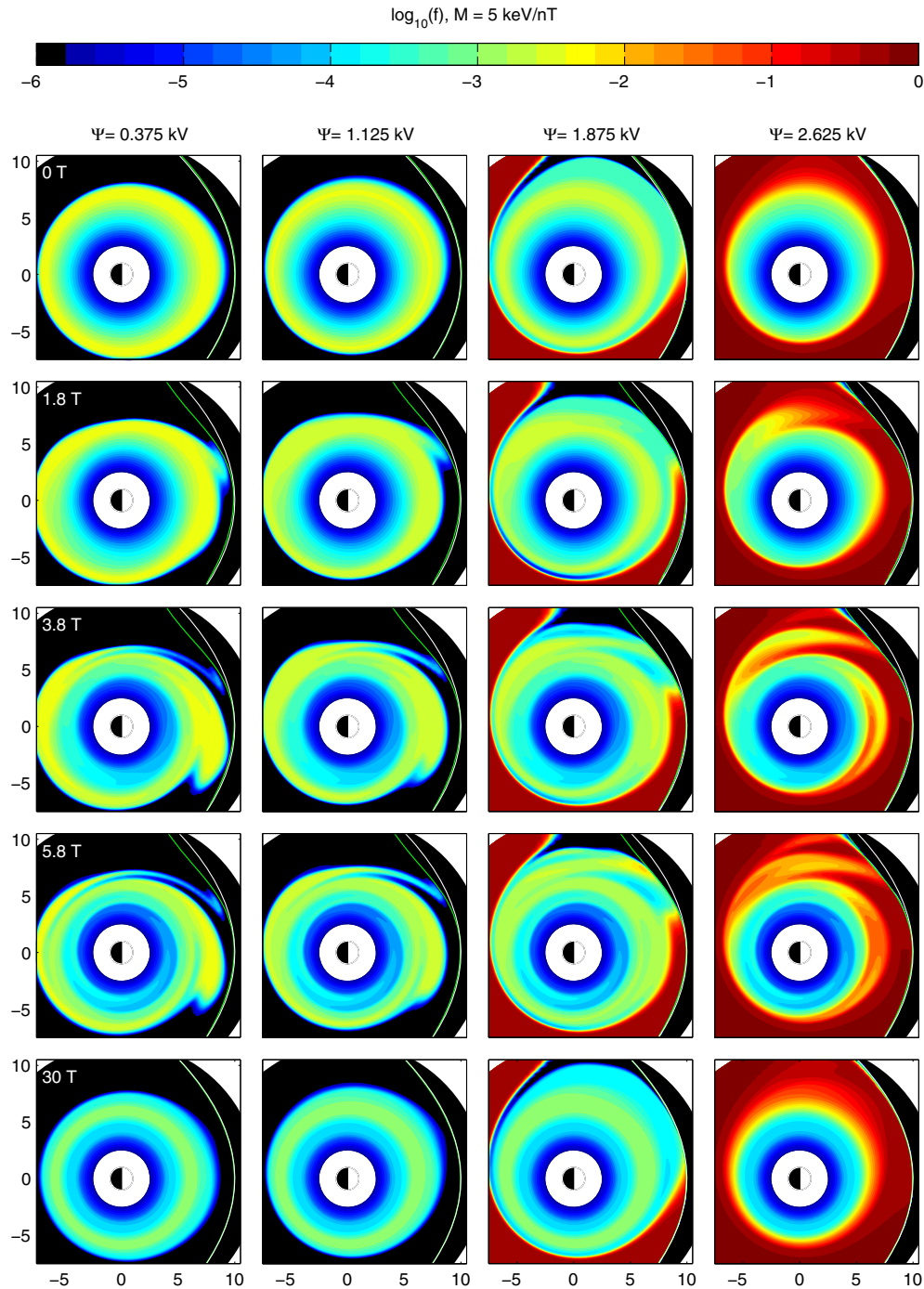


Figure 2. Still frames showing the log of the electron phase space density for equatorially mirroring electrons with $M = 5$ keV/nT. Each row corresponds to a different time-slice, as indicated in wave periods (T). Each column corresponds to a different convection electric field setting, with ψ_o increasing from 1.875 to 3 kV from left to right. The white and green curves in each plot respectively mark the equilibrium and perturbed magnetopause boundary (at the current time-slice).

40 wave periods (about 11 h, not shown in the figure). This allowed the system to equilibrate before the ULF wave source was activated, resulting in the distributions shown in the top row of the figure. Note that the first three cases show centrally peaked PSD distributions with L-shell. The subsequent rows in Figure 2 show the action of the ULF wave packet (in conjunction with the convection field) on

each distribution, with the frames in each row taken at intervals indicated (in wave periods). The bottom row shows the final distribution after the ULF wave packet has decayed to a negligible level, whereupon the PSD has returned to an equilibrium. These figures show the development of drift-resonant islands, with mixing between islands enhancing transport across L-shells, with periodic injections of PSD to

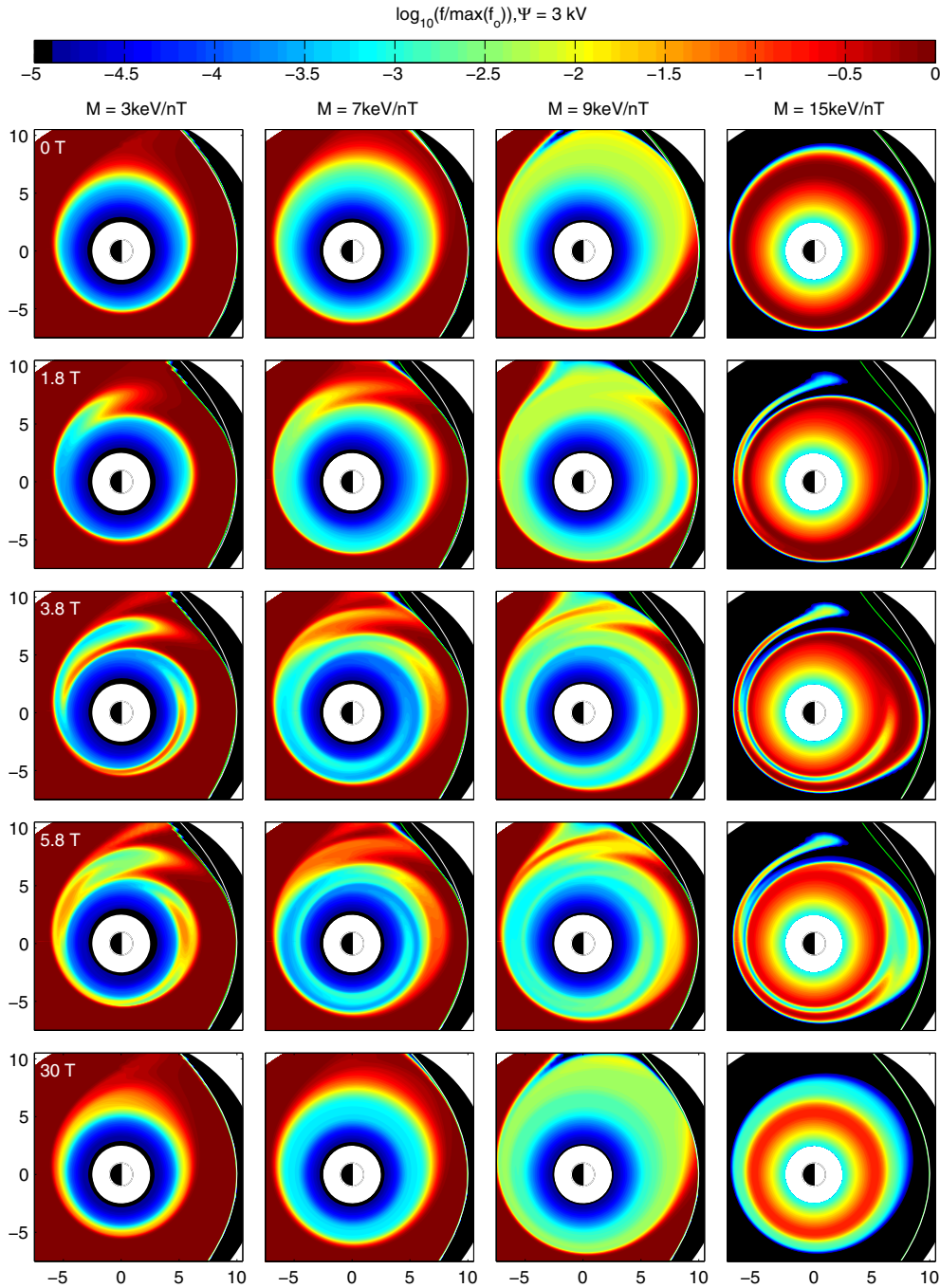


Figure 3. Still frames showing the log of the electron phase space density for equatorially mirroring electrons, for a convection electric field given by $\psi_o = 3 \text{ kV}$. Each row corresponds to a different time slice, as indicated in wave periods (T). Each column corresponds to a different first invariant M , increasing from 6 to 12 keV/nT from left to right.

lower L-shell, particularly in the afternoon sector. However, the three right-hand columns in this figure all show that there is no source population of electrons available for injection at high L-shell in the afternoon sector, but rather a distinct lack of PSD, or “PSD hole” due to magnetopause losses. These PSD holes become mixed with PSD at lower L-shell, and effectively lower the average PSD by multiple orders of magnitude in the 30 wave period interval shown (which corresponds to 8 h and 20 min).

[13] The effect of the convection electric field is clear, comparing the left and right-hand columns, starting with the top row. In the first and second columns from the left (low convection), the initial distribution shows a clear distinction between trapped and untrapped drift-orbiting electrons, with the untrapped electrons entirely absent from the frame, having already encountered the dawnside magnetopause. As the convection field is increased, the final point of departure of the untrapped electrons extends along the morning

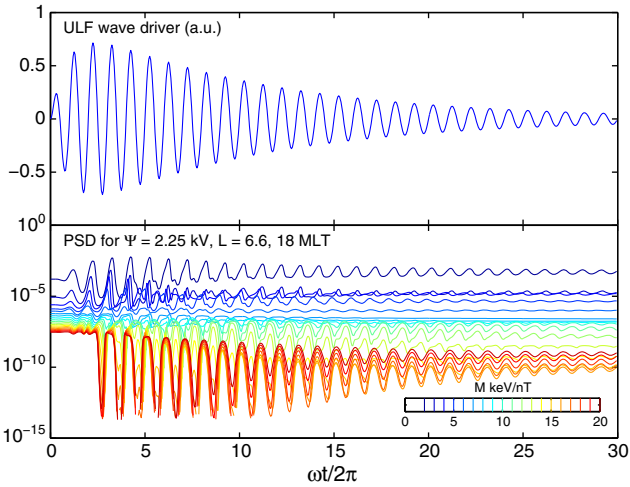


Figure 4. (a) The real part of the input signal used to drive the ULF wave source in all cases presented in this paper. (b) Time-series showing the variation in PSD with time for equatorially mirroring electrons with M between 2 and 20 keV/nT, sampled at the position $L = 6.6$, at 18 h MLT.

magnetopause towards the afternoon sector, becoming visible in the frame in the third column from the left. Most of these electrons remain untrapped, hence the final inner population resembles those of weaker convection field strength in

the left hand columns. In the far-right example, corresponding to the strongest convection field, the separatrix between trapped and untrapped orbits lies inside the magnetosphere, and a population of untrapped electrons extends across the entire dayside magnetosphere. In this case, as shown by subsequent rows in the right hand column, the untrapped electrons along the afternoon sector at high L -shell act as a source population for injection to lower L -shell. This results in an order of magnitude enhancement in the average PSD over the time interval shown.

[14] Figure 3 shows a series of model runs in which the magnetic moment is scanned from 2 to 20 keV/nT, keeping the ULF wave amplitude and convection fields unchanged. Note that the right-hand column, corresponding to the highest magnetic moment shown, has an initial equilibrium PSD distribution that is centrally peaked with L -shell. These plots show an enhancement in PSD due to ULF waves for low magnetic moments. However, there is a threshold between magnetic moments of 8 and 10 keV/nT above which the average PSD becomes more strongly depleted due to magnetopause shadowing. This threshold between enhancement and depletion is clearly shown by plotting the time-evolution of PSD at various magnetic moments, taken at $L = 6.6$ and 18 h MLT, as shown in Figure 4. In this figure, the top plot shows the ULF wave driver signal for reference, and the bottom plot shows the PSD evolution with time, in which coherent modulations at the wave period which respectively develop either a positive or negative bias

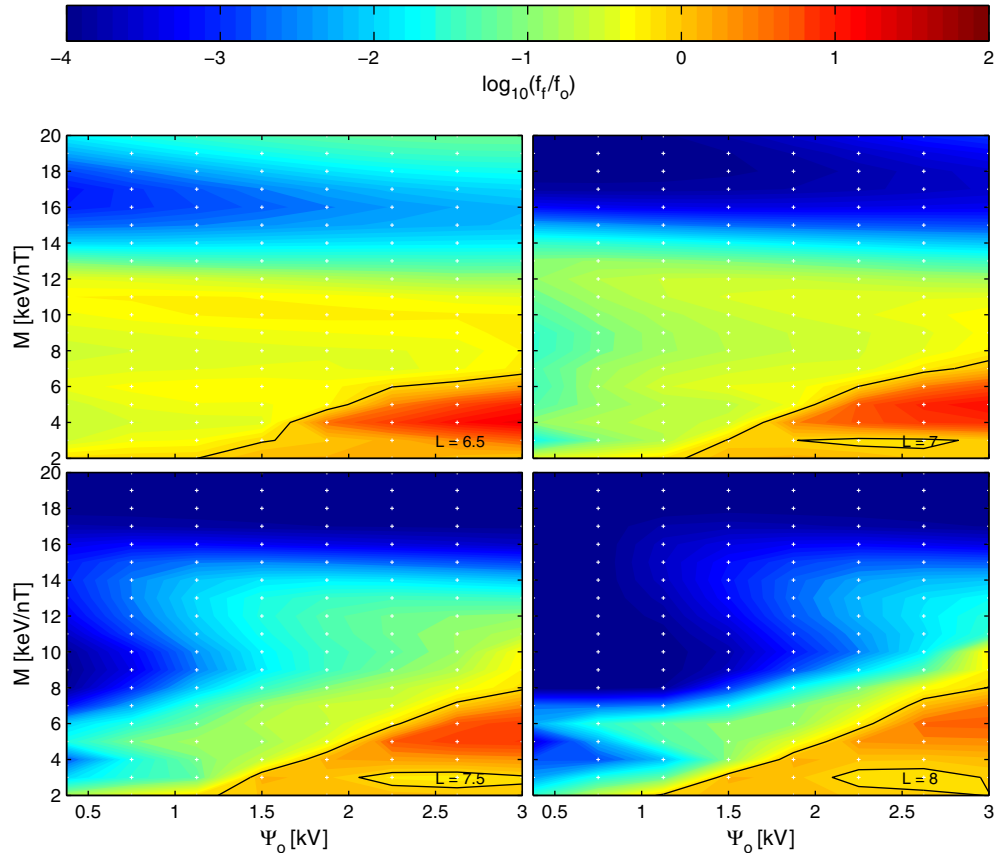


Figure 5. Log of the ratio of the MLT-average final PSD to the MLT-average initial PSD scanning M and ψ_o , at various L -shells from 6.5 to 8, for ULF waves launched from a source centered at 1500 h MLT (as in Figure 1). The zero-level contour, indicating no change in PSD, is shown as a solid black line.

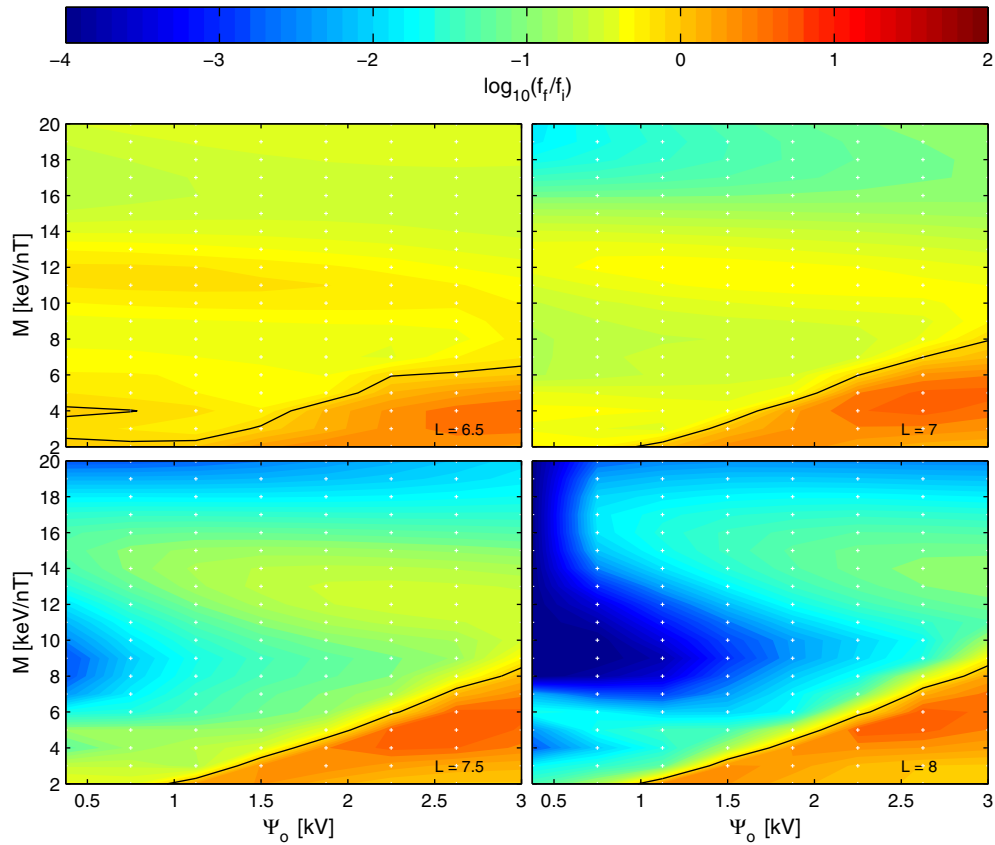


Figure 6. Log of the ratio of the MLT-average final PSD to the MLT-average initial PSD scanning M and ψ_o , at various L-shells from 6.5 to 8, for ULF waves launched from a source centered at 0900 h MLT (i.e., the reflection of the waves shown in Figure 1 about the noon-midnight meridian). The zero-level contour, indicating no change in PSD, is shown as a solid black line.

with time for the low and high M cases, indicating a net enhancement or dropout.

[15] The threshold relationship between magnetic moment and convection field strength is explored by comparing the ratio of the final to the initial PSD, for a series of parameter scans in ψ_o (from 0 to 3 kV) and M (from 2 to 20 keV/nT), using the same localized ULF wave source. The resulting ratios f_f/f_o at 18 h MLT and various L-shells are shown as functions of ψ_o and M in Figure 5 for ULF waves launched at 1500 h MLT, and Figure 6 for ULF waves launched at 0900 h MLT.

[16] For ULF waves launched in the afternoon sector, Figure 5 reveals a number of features in the ratio f_f/f_o that correspond to a strong dependence of PSD on M , ψ_o and L-shell. For example, for a strong convection electric field ($\psi_o = 3$ kV and $L = 6.5$) PSD becomes strongly depleted for magnetic moments above 8 keV/nT, and more so for lower M at weaker values of the convection electric field. There is also a dependence of PSD on L-shell, with the level of depletion increasing with L above a certain threshold value of M . The value of this threshold in M decreases smoothly with ψ_o , and reflects the increasing source (or shielding effect from magnetopause shadowing) of untrapped electrons that extends along the afternoon sector as the separatrix between trapped and untrapped electrons occurs at a lower L-shell. Below the threshold value of M , PSD is enhanced rather than depleted. Figure 6, corresponding to the scenario where ULF

waves of the same amplitude are launched from the morning sector, shows a much weaker dependence in the ratio f_f/f_o with M and ψ_o , (although similar trends in the data are visible) indicating a reduction in coupling between the electron dynamics and ULF wave activity. One might expect this is because the ULF waves launched from this location propagate mainly down the dawnside flank of the magnetosphere, in the opposite direction to the electron drift-orbital motion. However, E_ϕ shows predominantly standing wave character along the dayside magnetosphere in Figure 1, indicating the propagation of power in both directions. This suggests that the proximity of the ULF wave source location to the afternoon sector (i.e., allowing accessibility of ULF perturbations to the separatrix region between trapped and untrapped orbits) is also a determining factor.

4. Model Comparison With Observations

[17] As a first step towards searching for evidence that ULF wave-driven electron transport can result in a dropout in electron phase space density, we took the database of 52 events from *Green et al.* [2004], and searched for cases where the Churchill line of Canadian ground-based magnetometers were on the dayside, and measured significant ULF activity within 2 h prior to the recorded time of the dropout. Of the original set, a total of 38 events occurred with the Churchill line located on the dayside, however,

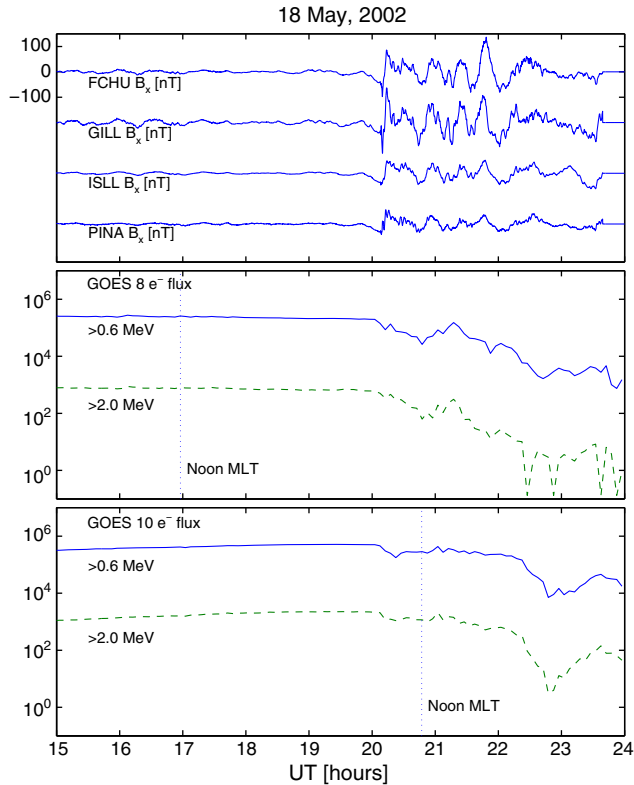


Figure 7. (a) Detrended H-component of the magnetic field measured at Gillam and (b) GOES 8 and 9 > 0.6 and > 2.0 MeV integrated electron flux, for event 59 of the event list in *Green et al.* [2004].

most of these events did not show any correlation in timing with ULF wave activity. There were four events, however, which did show a correlation in timing between Churchill line ULF wave activity and a subsequent dropout (event numbers 5, 25, 48 and 59 from the published list) in GOES satellite (> 0.6 or > 2.0 MeV) integrated electron flux. In each of these cases, the ULF wave spectrum was peaked at or below 1 mHz. An interesting example (event 59) is shown in Figure 7. This figure shows 0.2 mHz low-pass filtered time series from Fort Churchill, Gillam, Island Lake and Pinawa magnetometers (GCM Latitudes 68.99, 66.69, 64.26 and 60.56; GCM longitudes 332.38, 331.58, 332.32 and 330.76, respectively). These signals show ULF wave activity across a wide range in L, starting at 20 h UT, at which time GOES 8, located at 15 h MLT, shows the initiation of a decreasing trend in > 0.6 and > 2.0 MeV integrated flux, lasting for the next 4 h. Meanwhile, GOES 10 is located at 11.10 MLT at the time of ULF onset, and shows a significant, very rapid dropout between 22.20 and 22.45 UT (for both > 0.6 and > 2.0 MeV integrated flux), at which point the satellite is located between 13.30 and 13.55 MLT. Although electron flux contains adiabatic variations whereas PSD does not, the delay in the dropout seen in GOES 10 compared to GOES 8, combined with the more rapid depletion seen on GOES 10 compared to GOES 8, may indicate that GOES 10 passes through the MLT location where PSD holes have recently been (or are being) injected from the magnetopause by the ULF wave activity. GOES 8, on the other hand, is already

well into the afternoon sector at the onset time of ULF wave activity, and may be seeing the anti-sunward drift of the PSD holes arriving at its location.

5. Conclusion

[18] In this article, we have studied the process of magnetospheric radiation belt electron transport driven by ULF waves and a simple model of the convection electric field, including a nightside plasma sheet source and losses by magnetopause shadowing. We find that ULF waves launched from a spatially localized source on the dayside magnetosphere provide a mechanism for rapid enhancement of electron phase space density for cases of strong magnetospheric convection (e.g., $E_{\text{conv}} \approx 5$ mV/m) and relatively low values of the first adiabatic invariant (e.g., $M < 8$ keV/nT). For higher magnetic moments and weaker convection, ULF waves can cause a rapid depletion of PSD by orders of magnitude, across a range of L-shells, by magnetopause shadowing losses, and the transport of PSD holes across the magnetopause into the magnetosphere. In either case, the ULF wave-driven transport, and hence the magnitude and extent in L-shell of the PSD enhancement or depletion, is strongly dependent on the amplitude of ULF waves in the afternoon sector, and is significantly augmented by the overlap of drift-resonant islands and an associated stochastic transport layer. The ULF waves included in the model presented are primarily poloidal mode compressional waves, with toroidal mode structure where the compressional mode couples in the inner magnetosphere to field line resonances. The importance of the poloidal mode has been pointed by *Zong et al.* [2007, 2009], but a detailed analysis is deferred to a future study.

[19] **Acknowledgments.** The authors would like to thank I.R. Mann, D.K. Milling, and the CARISMA team for the provision of CARISMA magnetometer data (CARISMA is operated by the University of Alberta and funded by the Canadian Space Agency). We also thank M. Gordon and the CESWP team for their enthusiastic computing infrastructure support. This work is partially funded by the Canadian Space Agency, Natural Sciences and Engineering Research Council of Canada, and the U.S. National Science Foundation.

References

- Allan, W., and F. Knox (1979), Effect of finite ionosphere conductivities on axisymmetric toroidal Alfvén wave resonances, *Planet. Space Sci.*, *27*(7), 939–950.
- Allan, W., and F. Poulter (1992), ULF waves—their relationship to the structure of the Earth's magnetosphere, *Rep. Prog. Phys.*, *55*, 533–598.
- Brautigam, D., and J. Albert (2000), Radial diffusion analysis of outer radiation belt electrons during the October 9, 1990, magnetic storm, *J. Geophys. Res.*, *105*(A1), 291–309, doi:10.1029/1999JA900344.
- Chen, Y., G. D. Reeves, and R. H. W. Friedel (2007), The energization of relativistic electrons in the outer Van Allen radiation belt, *Nature*, *3(9)*, 614–617, doi:10.1038/nphys655.
- Degeling, A. W., and R. Rankin (2008), Resonant drift echoes in electron phase space density produced by dayside Pc5 waves following a geomagnetic storm, *J. Geophys. Res.*, *113*(A10), doi:10.1029/2008JA013254.
- Degeling, A. W., R. Rankin, and S. R. Elkington (2011), Convective and diffusive ULF wave driven radiation belt electron transport, *J. Geophys. Res.*, *116*, doi:10.1029/2011JA016896.
- Friedel, R., G. Reeves, and T. Obara (2002), Relativistic electron dynamics in the inner magnetosphere a review, *J. Atmos. Sol. Terr. Phys.*, *64*(2), 265–282, doi:10.1016/S1364-6826(01)00088-8.
- Green, J. C., and M. G. Kivelson (2004), Relativistic electrons in the outer radiation belt: Differentiating between acceleration mechanisms, *J. Geophys. Res.*, *109*, doi:10.1029/2003JA010153.

- Green, J. C., T. G. Onsager, T. P. O'Brien, and D. N. Baker (2004), Testing loss mechanisms capable of rapidly depleting relativistic electron flux in the earth's outer radiation belt, *J. Geophys. Res.*, *109*, doi:10.1029/2004JA010579.
- Hudson, M. K., B. T. Kress, H.-R. Mueller, J. A. Zastrow, and J. B. Blake (2008), Relationship of the Van Allen radiation belts to solar wind drivers, *J. Atmos. Sol. Terr. Phys.*, *70*(5), 708–729, doi:10.1016/j.jastp.2007.11.003.
- Koller, J., Y. Chen, G. D. Reeves, R. H. W. Friedel, T. E. Cayton, and J. A. Vrugt (2007), Identifying the radiation belt source region by data assimilation, *J. Geophys. Res.*, *112*(A6), doi:10.1029/2006JA012196.
- Loto'aniu, T. M., H. J. Singer, C. L. Waters, V. Angelopoulos, I. R. Mann, S. R. Elkington, and J. W. Bonnell (2010), Relativistic electron loss due to ultralow frequency waves and enhanced outward radial diffusion, *J. Geophys. Res.*, *115*, doi:10.1029/2010JA015755.
- Northrop, T. G. (1963), *The Adiabatic Motion of Charged Particles*, chap. 3, pp. 42–67, Interscience Publishers, New York.
- O'Brien, T., R. McPherron, D. Sornette, G. Reeves, R. Friedel, and H. Singer (2001), Which magnetic storms produce relativistic electrons at geosynchronous orbit?, *J. Geophys. Res.*, *106*(A8), 15,533–15,544, doi:10.1029/2001JA000052.
- Rankin, R., K. Kabin, and R. Marchand (2006), Alfvénic field line resonances in arbitrary magnetic field topology, *Adv. Space Res.*, *38*(8), 1720–1729, doi:10.1016/j.asr.2005.09.034.
- Samson, J. C., J. A. Jacobs, and G. Rostoker (1971), Latitude-dependent characteristics of long-period geomagnetic micropulsations, *J. Geophys. Res.*, *76*, 3675–3683.
- Shprits, Y., D. Kondrashov, Y. Chen, R. Thorne, M. Ghil, R. Friedel, and G. Reeves (2007), Reanalysis of relativistic radiation belt electron fluxes using CRRES satellite data, a radial diffusion model, and a Kalman filter, *J. Geophys. Res.*, *112*(A12), doi:10.1029/2007JA012579.
- Shprits, Y., M. Daae, and B. Ni (2012), Statistical analysis of phase space density buildups and dropouts, *J. Geophys. Res.*, *117*, A01219, doi:10.1029/2011JA016939.
- Shue, J.-H., J. K. Chao, H. C. Fu, C. T. Russell, and P. Song (1997), A new functional form to study the solar wind control of the magnetopause size and shape, *J. Geophys. Res.*, *102*, 9497–9511.
- Stern, D. P. (1975), The motion of a proton in the equatorial magnetosphere, *J. Geophys. Res.*, *80*, 595.
- Turner, D. L., and X. Li (2008), Radial gradients of phase space density of the outer radiation belt electrons prior to sudden solar wind pressure enhancements, *Geophys. Res. Lett.*, *35*, 18, doi:10.1029/2008GL034866.
- Turner, D. L., X. Li, G. D. Reeves, and H. J. Singer (2010), On phase space density radial gradients of Earth's outer-belt electrons prior to sudden solar wind pressure enhancements: Results from distinctive events and a superposed epoch analysis, *J. Geophys. Res.*, *115*, doi:10.1029/2009JA014423.
- Turner, D. L., V. Angelopoulos, Y. Shprits, A. Kellerman, P. Cruce, and D. Larson (2012a), Radial distributions of equatorial phase space density for outer radiation belt electrons, *Geophys. Res. Lett.*, *39*, doi:10.1029/2012GL051722.
- Turner, D. L., Y. Shprits, M. Hartinger, and V. Angelopoulos (2012b), Explaining sudden losses of outer radiation belt electrons during geomagnetic storms, *Nat. Phys.*, *8*(3), 208–212, doi:10.1038/NPHYS2185.
- Volland, H. (1973), A semi-empirical model of large-scale magnetospheric electric fields, *J. Geophys. Res.*, *78*, 171.
- West, H., J. Walton, and R. Buck (1972), Shadowing of electron azimuthal-drift motions near noon magnetopause, *Nat. Phys. Sci.*, *240*(97), 6–8.
- Wygant, J., D. Rowland, H. J. Singer, M. Temerin, and M. K. MoHudson (1998), Experimental evidence on the role of the large spatial scale electric field in creating the ring current, *J. Geophys. Res.*, *103*(A12), 29,527–29,544.
- Zong, Q.-G., et al. (2007), Ultralow frequency modulation of energetic particles in the dayside magnetosphere, *Geophys. Res. Lett.*, *34*(12), doi:10.1029/2007GL029915.
- Zong, Q.-G., et al. (2009), Energetic electron response to ULF waves induced by interplanetary shocks in the outer radiation belt, *J. Geophys. Res.*, *114*, doi:10.1029/2009JA014393.